Quantitative Analysis of Susceptibility Effects in TRFGE and CGE Sequences for Functional MRI

S.C. Chung[1], Y.M. Ro[2], Z.H. Cho[1]

fMRI, functional MRI introduced recently appears based on the gradient echo technique which is sensitive to the field inhomogeneity developed due to the local susceptibility changes of blood oxygenation and deoxygenation. There has been many variants of the basic gradient echo sequence which is sensitive to the local inhomogeniety, among others such as GRASS or SSFP to EPISTAR are the most commonly used gradient echo techniques. Common to all these gradient echo techniques is that the signal due to the susceptibility effects is generally decreased with increasing inhomogeneity due to the T2* effect or conventionally known as blood oxygenation level dependent (BOLD) effect. It is, also found that the BOLD sensitivity is also dependent on the imaging modes, namely whether the imaging is in axial, or coronal or sagittal mode as well as the directions of the vessels against the main magnetic field. We have, therefore, launched a systematic study of imaging mode dependent signal change or BOLD sensitivity as well as the signal changes due to the tilting angle of the imaging planes. Study has been made for both TRFGE sequence and CGE sequence to compare the distinctions of the each mode since each technique has different sensitivity against susceptibility effect. Method of computation and both the computer simulations and their corresponding experimental results are presented.

Index words : fMRI ; susceptibility effect ; imaging mode ; tilting angle

Introduction

Functional MRI based on the susceptibility effect and deoxygenated blood relies on the gradient echo imaging or similar techniques (1−11), such as the tailored RF gradient echo technique which we termed as TRFGE technique (12−16).

Questions raised in CGE as well as TRFGE techniques in fMRI are, however, the generality of the methods in quantitative assessment of the susceptibility effect or susceptibility difference as a function of parameters involved in the techniques, such as the echo times, repetition times, flip angles, and thickness of the slice selected and angles of the imaging slices or vessels against the main static magnetic field, B_0 as well as the imaging modes, whether the imaging mode is axial, coronal, or sagittal. Especially the latters, i.e., the angle of imaging slices, or vessels in relation to the imaging mode are closely related to the signal strength resulting from the susceptibility effect that could be developed in the imaging sequence. It is, therefore, important to investigate accurately how those slice tilting angle of

JKSMRM 1 : 66−74(1997)

[1] Department of Electrical Engineering, KAIST, Seoul
[2] Department of Computer Engineering, Taejon University, Taejon
Address reprint requests to : Soon-Cheol, Chung, Ph.D., Dept. of Electrical Engineering, KAIST, 207-43 Cheongryangni-Dong, Dongdaemun-Gu, Seoul, Korea. Tel. 82-2-958-3352 Fax. 82-2-965-4394

the imaging slices as well as the vessels against main field affect the sensitivity of the measurements. In this paper, both experiments and computer simulations are carried out for various forms of vessels raging from a single cylinder to a bundle of capillaries tilted against main field at three different imaging modes (axial, coronal and sagittal). To observe the effects on fMRI application, both CGE and TRFGE sequences are studied and compared the results, and attempted to analyze quantitatively the susceptibility effects on fMRI.

Theory

1. Magnetic Fields and Susceptibility Effect

To study the distortion of the main magnetic field from the susceptibility difference between interior and exterior of a blood vessels of different sizes, a cylinder (or capillary) is placed at the middle of a large tube filled with water and tilted to the main field, as shown in Fig. 1. The magnetic field can be calculated from magnetic potential equation which is a Laplacian equation given in Eq. [1].

$$\frac{1}{r}\frac{\partial}{\partial r}\left(r\frac{\partial V}{\partial r}\right)+\frac{1}{r^2}\frac{\partial^2 V}{\partial \varphi^2}+\frac{\partial^2 V}{\partial y^2}=0, \qquad [1]$$

where r, y, and φ are the standard cylindrical coordinates and angles, and $V(r, \varphi, y)$ is the magnetic potential, respectively. Using the method of separation of variables, the magnetic potential, $V(r, \varphi, y)$ can be written as,

$$V(r, \varphi, y)=R(r)\Phi(\varphi)Y(y), \qquad [2]$$

where R(r) is function of variable r, $\Phi(\varphi)$ is function of φ and Y(y) is function of y, respectively. By replacing V in Eq. [1] with Eq. [2] and with some calculations, following results are obtained,

$$\Phi(\varphi)=A_\varphi \cos\varphi+B_\varphi \sin\varphi, \qquad [3]$$

$$\frac{1}{rR(r)}\frac{dR}{dr}-\frac{1}{R(r)}\frac{d^2R}{dr^2}-\frac{1}{r^2}=m^2,$$

$$\text{and } \frac{1}{Y(y)}\frac{\varphi^2 Y}{\varphi y^2}=-m^2$$

where A_φ and B_φ are the coefficients which can be

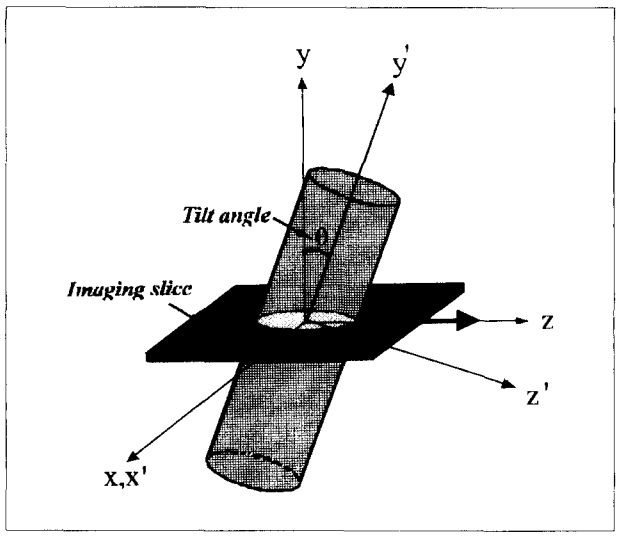

Fig. 1. The tilting cylinder against the main field, B_0

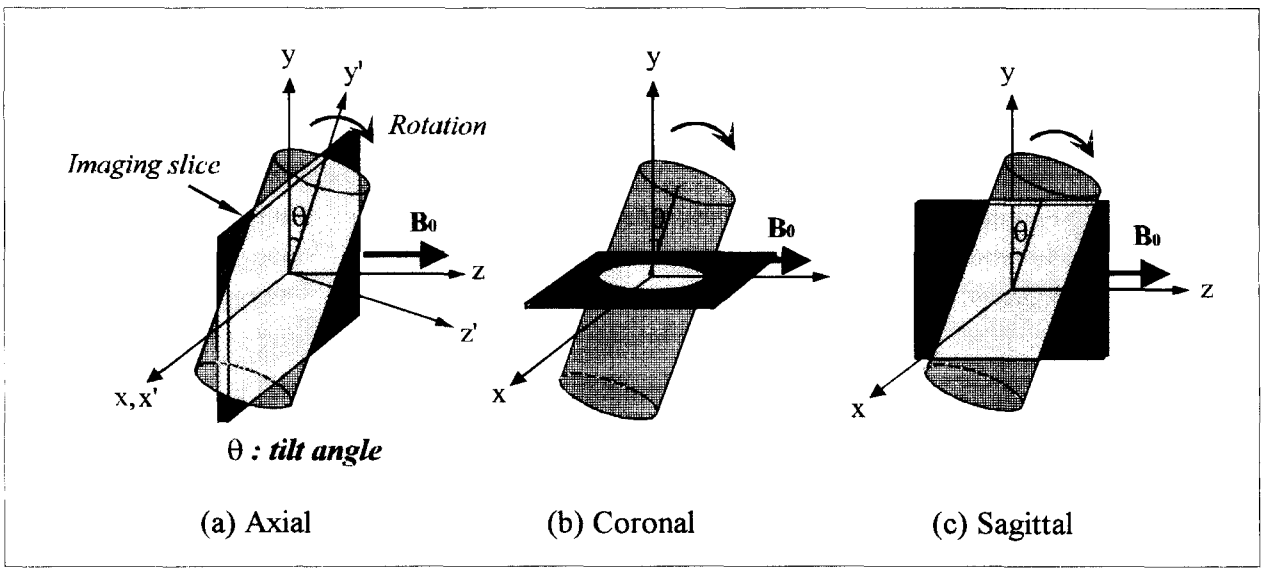

Fig. 2. Three different imaging modes or views of a cylinder which is a simple tube or a bundle of vessels or small capillaries with tilting an angle θ against the main magnetic field (namely axial, coronal, and sagittal).

evaluated from the boundary conditions. From Eq. [3], the transverse and vertical components of the main field can be obtained separately.

In Fig. 2, three views, namely axial, coronal and sagittal imaging planes or views are shown with a tilt angle θ. The cylinder is a simple tube or a bundle consists of vessels or small capillaries. For each imaging mode, tilt angle is varied between 0° to 90° and measured magnetizations at all points on each plane, namely axial(xy), coronal(zx), and sagittal (yz), and calculated $B_{x'}$, $B_{y'}$ and $B_{z'}$.

2. Signal Obtainable with CGE and TRFGE for the Susceptibility Affected Voxel

a. Signal Intensity and the Susceptibility Effect

The signal intensity from a voxel surrounded by materials having different magnetic susceptibilities is reduced due to spin dephasing within the voxel. Let us first analyze the relationship between the intravoxel signal intensity and the phase distribution generated by the susceptibility effect. Consider a voxel whose spins are distributed according to the field variation due to the susceptibility effect and assume that the slice thickness (along the z-direction) is relatively thin so that the fields induced within each voxel are linear. In this circumstance the phases of the spins in the voxel will be distributed linearly, that is, the spin phases become either incoherent or dephased, otherwise inphased, under the constant field. The phase distribution in the slice selection direction (z-direction) due to the susceptibility-induced field variation in gradient echo imaging can then be given as

$$\theta_{sus}(z)=\gamma T_E G_{sus} z$$
$$\text{or} \quad =P_{sus} z \qquad [4]$$

where γ is the gyromagnetic ratio, T_E is the echo time, G_{sus} is the field gradient created by the susceptibility difference between the paramagnetic substance and the surrounding tissue, z is the position in the selected slice, and P_{sus} is the phase gradient induced by the susceptibility effect, i.e.,

$$P_{sus}=\gamma T_E G_{sus} \qquad [5]$$

This phase gradient is a result of the combined effects of susceptibilities within both a voxel and a pulse sequence and is and externally controllable parameter.

b. Conventional Gradient Echo (CGE) Imaging.

As is know the RF pulse used in conventional gradient echo imaging is a sinc shaped pulse and has a constant phase distribution in the slice-selection direction. Therefore, the actual phase distribution developed along the slice-selection direction within the voxel is more or less dictated by the existing field in the voxel, such as the susceptibility-induced field. In other words, a constant phase distribution will develop for the normal tissue but a strong linear phase distribution will develop in a voxel affected by susceptibility. In the latter, the spins are affected by the linear gradient due to the susceptibility and their phases will be dephased, resulting in intravoxel signal attenuation. The intravoxel signal, S as a function of the susceptibility-induced phase gradient can then be written as

$$S=\left| \int_{-\infty}^{+\infty} M \, \text{rect}\left(\frac{z}{z_0}\right) \exp(iP_{sus} z)dz \right| \qquad [6]$$

where M is the magnetization, z_0 is the slice thickness, and rect(z/z_0) is the rectangular function with a width of z_0. In this case, we have assumed that resolutions in the transverse (x, y) directions are much higher than the resolution in the slice-selection direction (z) and it is also normalized so that the signal from the voxel is simply the integration of the magnetizations within the selected slice thickness. By Fourier transform, under the assumption that P_{sus} is a variable, Eq. [6] can be rewritten as

$$S=Mz_0 \left| \, \text{sinc}\left(\frac{P_{sus}}{2\pi} z_0\right) \right| \qquad [7]$$

According to Eq. [7], the intravoxel signal decreases with increasing phase gradient (P_{sus}) and in addition signal voids are present at each phase gradient of $\pm 2\pi N/z_0$ where N is an integer. This means that the image contrast is strongly affected by susceptibility. Consequently, if gradient echo imaging is used, the susceptibility effect will appear as a signal vold or a dark area because of this intravoxel signal attenuation. The signal loss due to the susceptibility effect will be particularly visible, for example in the interfaces between the air and normal surrounding tissues or deoxygenated blood (venous blood) or venous capillary beds and normal tissue. The resulting

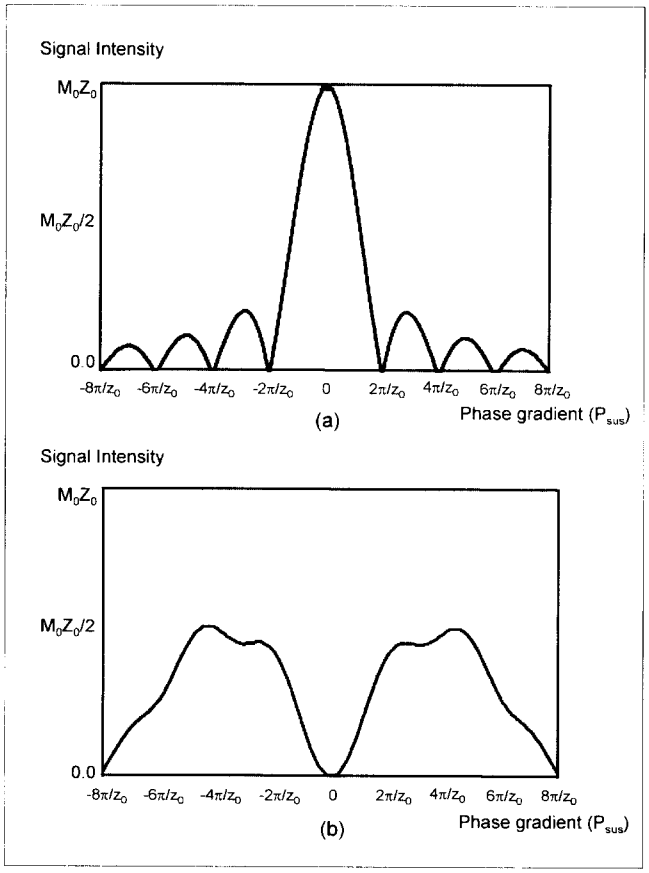

Fig. 3. Signal intensity distributiona as a function of the susceptibility phase gradient P_{sus}, when (**a**) a conventional sinc-shaped RF pulse is applied. (**b**) a tailored RF pulse with a bilinear saw-tooth-like phase distribution in the selected slice is applied.

image will then be attenuated due to the strong local field gradients produced at these interfaces. This signal attenuation is the bases of T2* attenuation utilized in fMRI with Conventional Gradient Echo (CGE) sequence and it's variation.

c. Tailored RF Gradient Echo (TRFGE) Imaging

As briefly mentioned above, the phase distribution of the spins in a voxel which affect signal intensity can now be modified by the externally applied slice-selection RF pulse. In conventional NMR imaging, the slice-selection RF pulse is in the form of a sinc function which has no particular phase distribution within the selected slice, i.e., a constant phase distribution in the slice-selection direction. A normal sinc RF pulse in conventional gradient echo imaging, therefore, dose not affect the spin phase distribution of the intravoxel spins originally developed within the selected slice.

Let us now assume that a tailored RF pulse with phase distribution $\theta_{RF}(z)$ in the slice-selection direction is added to the existing phase distribution $\theta_{sus}(z)$: the total phase distribution of the intravoxel spins then becomes $\theta_{total}(z)=\theta_{sus}(z)+\theta_{RF}(z)$. The signal from the voxel then appears as

$$S=\left|\int_{-\infty}^{+\infty} M \text{ rect}\left(\frac{z}{z_0}\right) \exp[i\theta_{total}(z)]dz\right| \quad [8]$$

or

$$S=\left|\int_{-\infty}^{+\infty} M \text{ rect}\left(\frac{z}{z_0}\right) \exp[i\theta_{RF}(z)] \exp[iP_{sus}\cdot z]dz\right| \quad [9]$$

Using P_{sus} as a variable, Eq.[9] can be expressed as a Fourier transform relation, i.e.,

$$S=\left| 2\pi \text{ MF}^{-1}\left[\text{rect}\left(\frac{z}{z_0}\right) \exp[i\theta_{RF}(z)\right]\right|, \quad [10]$$

or

$$S=\left| 2\pi \text{ Mz}_0 \text{ sinc}\left(\frac{P_{sus}}{2\pi} z_0\right) * F^{-1}[\exp[i\theta_{RF}(z)]]\right|, \quad [11]$$

where F^{-1} represents the 1D inverse Fourier transform operator, and * represents the convolution operator. This result indicates that the signal intensity given as a function of the strength of the susceptibility-induced phase gradient can be altered by an externally applied tailored RF pulse to a desired total phase distribution, i.e., altering the spin phase distribution within a voxel so that it could result in either an enhanced signal or a further attenuated signal.

To accomplish this goal, a tailored RE pulse with a phase distribution similar to a bilinear saw-tooth-like distribution is chosen. Resulting spin phases then distribute uniformly from 0 to 2π rad ($\theta_{RF}(z)=4\pi|z|/z_0$) along the slice-selection direction. The corresponding signal intensity then becomes

$$S=\left| 2\pi \text{ M } z_0 \text{ sinc}\left(\frac{P_{sus}}{2\pi} z_0\right) * F^{-1}\left[\exp\left(i\frac{4\pi|z|}{z_0}\right)\right]\right|, \quad [12]$$

Figures 3a and 3b show signal intensity of obtained by conventional gradient echo (CGE) sequence and tailored RF gradient echo (TRFGE) sequence, respectively. As shown in Fig. 3, in normal tissue where $P_{sus}=0$ no signal is produced : therefore. signal suppression is achieved for the normal tissues. However, since the signal intensity increases monotonically with increasing phase gradient (up to $\pm 4\pi/z_0$), the signal intensity increases as the susceptibility-induced phase gradient increases. Conse-

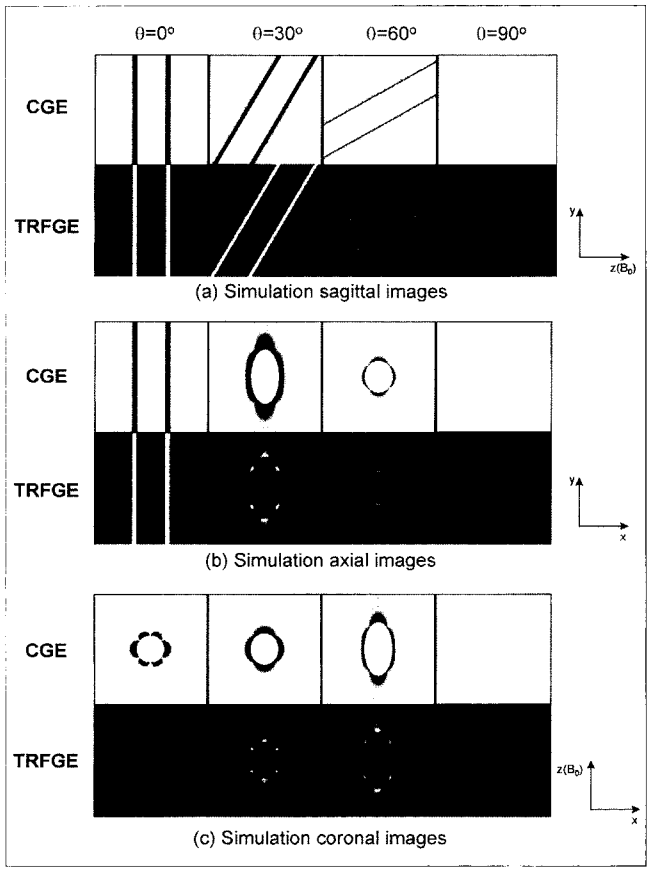

Fig. 4. Simulation images of a single cylinder with the CGE and TRFGE sequences, respectively for four tilting angles.

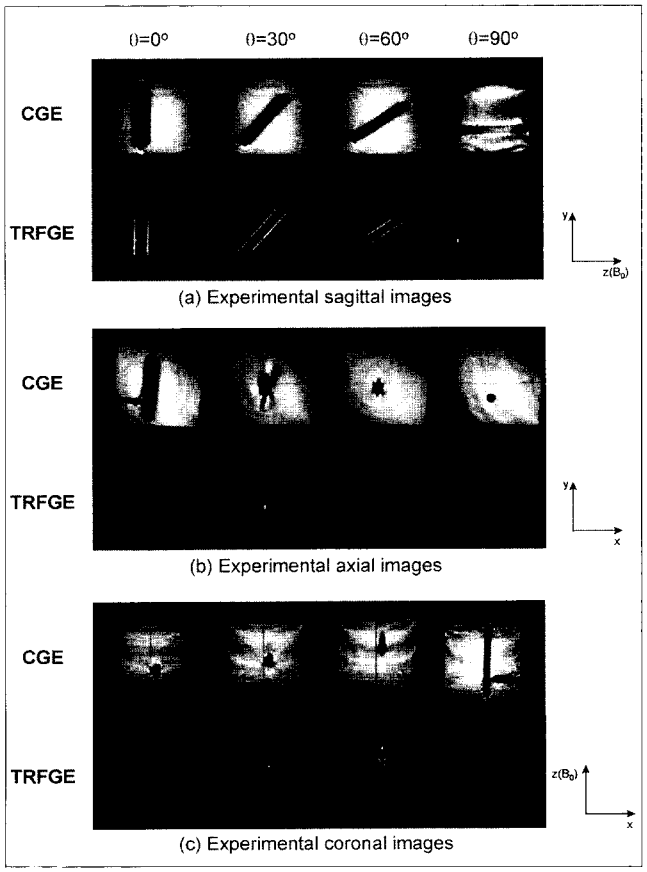

Fig. 5. Experimental images of a single cylinder with the CGE and TRFGE sequences, respectively for four tilting angles.

quently, this tailored RF pulse can, therefore, effectively be used to enhancing the signals from the blood-tissue interfaces where the susceptibility effect is high, for example, due to the deoxygenated blood or deoxyhemoglobin while suppress the signals form normal tissues.

3. Susceptibility Effect in Blood

The volume susceptibility of a bulk deoxygenated blood was known to be 0.08ppm at 2 Tesla (17). Using oxygenation of the hemoglobin, the magnetic susceptibility difference in blood can be written as;

$$\chi_{v,\,blood}(Y)=(1-Y)\,\Delta\chi^{o}_{v,\,blood} \qquad [12]$$

where Y is the fraction of oxygenated hemoglobin. For human, the fraction of oxygenated hemoglobin Y can be calculated from the blood oxygenated curve which is given as (18)

$$\frac{Y}{1-Y}=\left(\frac{pO_2}{P_{50}}\right)^{2.8} \qquad [13]$$

where pO_2 is the partial pressure of oxygen in the blood and P_{50} is the partial pressure of oxygen at which half of the hemoglobin sites are bound (P_{50}=26torr). Assuming partial oxygen pressure in capillaries varies between 20 and 40torr where 20torr corresponds to the normal stage while 40torr corresponds to the stimulated or oxygen rich state, respectively (19). Then the susceptibility difference indicates a corresponding value of 0.05ppm using Eq. [12] and [13]. These values are used for the both simulation and experimental studies.

Experimental Results and Computer Simulations

Computer simulations and experiments are carried out for a single cylinder as well as bundles of capillaries with different capillary sizes. The cylinder or bundles then varied the tilting angle against the main field, B0 for the axial, coronal and sagittal imagings or views, respectively (see Fig. 2). For the single cylinder experiments, a cylinder of diameter

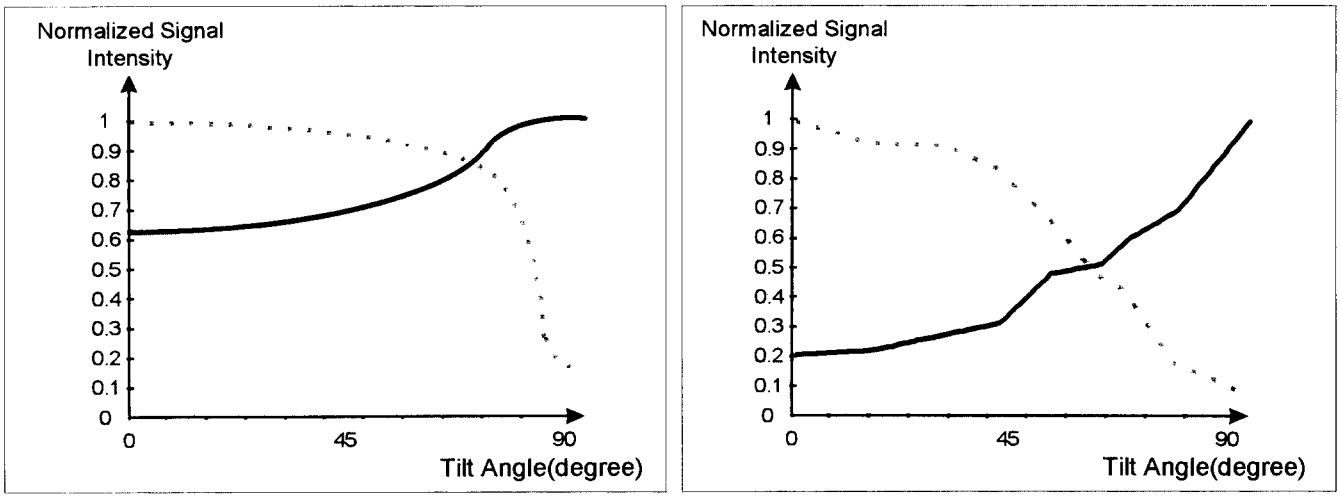

a Simulation result
CGE sequence ———
TRFGE sequence --------

b Experimental result

Fig. 6. Normalized signal intensity changes as a function of the tilting angle for sagittal views with the CGE and TRFGE sequences, respectively.
a. Simulation result.
b. Experimental result.

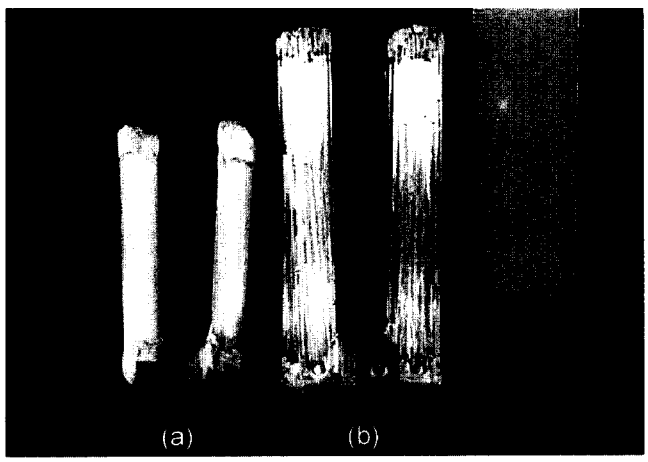

Fig. 7. For the capillary experiments, a 15mm diameter bundle consists of 1mm diameter tubes and 10mm diameter bundle with 300μm diameter tubes lumped together are used. Also two capillary bundles with two different susceptibility values, namely 20mM and 18mM Gd—DTPA solutions are used to measure the contrast sensitivity.
a. 10mm diameter bundles, each with 200 pieces of 300μm diameter tube.
b. 15mm diameter bundles, each with 40 pieces of 1mm diameter tube.

of 1mm, 5mm and 10mm, respectively is used. The cylinder is filled with diluted Gd—DTPA solution (10mM). Imaging parameters are TR/TE=40/25 msec, flip angle α=16° and slice thickness=5mm for both CGE and TRFGE sequences. Normalized signal intensity changes are observed with varying the tilting angle for three different imaging modes were simulated and results shown in Fig. 4(a), (b), and (c) and its corresponding experimental counterparts are also shown in Fig. 5(a), (b), and (c), respectively. These images are obtained by both with single cylinder for CGE and TRFGE sequences. Fig. 6 is the normalized signal intensity changes as a function of the tilting angle θ for sagittal views for both simulated and experimental data are shown for comparison. Although there is some differences between the simulations and experiments, the trends of variation appear same for two cases. The signal intensity changes a more or less opposite as expected for CGE and TRFGE. When the cylinder is perpendicular to the main field the susceptibility effect is maximized. Therefore, the signal intensity of the TRFGE sequence is maximized. When the cylinder gradually tilted, the susceptibility effect is also gradually decreased. The experimental results, however, show relative advantage of the TRFGE, having relatively large signal intensity over the tilt angles.

More crucial and mimicking the true situation is experiments with small capillary tube bundles. For the capillary bundle experiments, a 15mm diameter bundle consists of 40 pieces of 1mm diameter tubes and 10mm diameter bundle with 200 pieces of 300μm diameter tubes lumped together are used (see Fig.

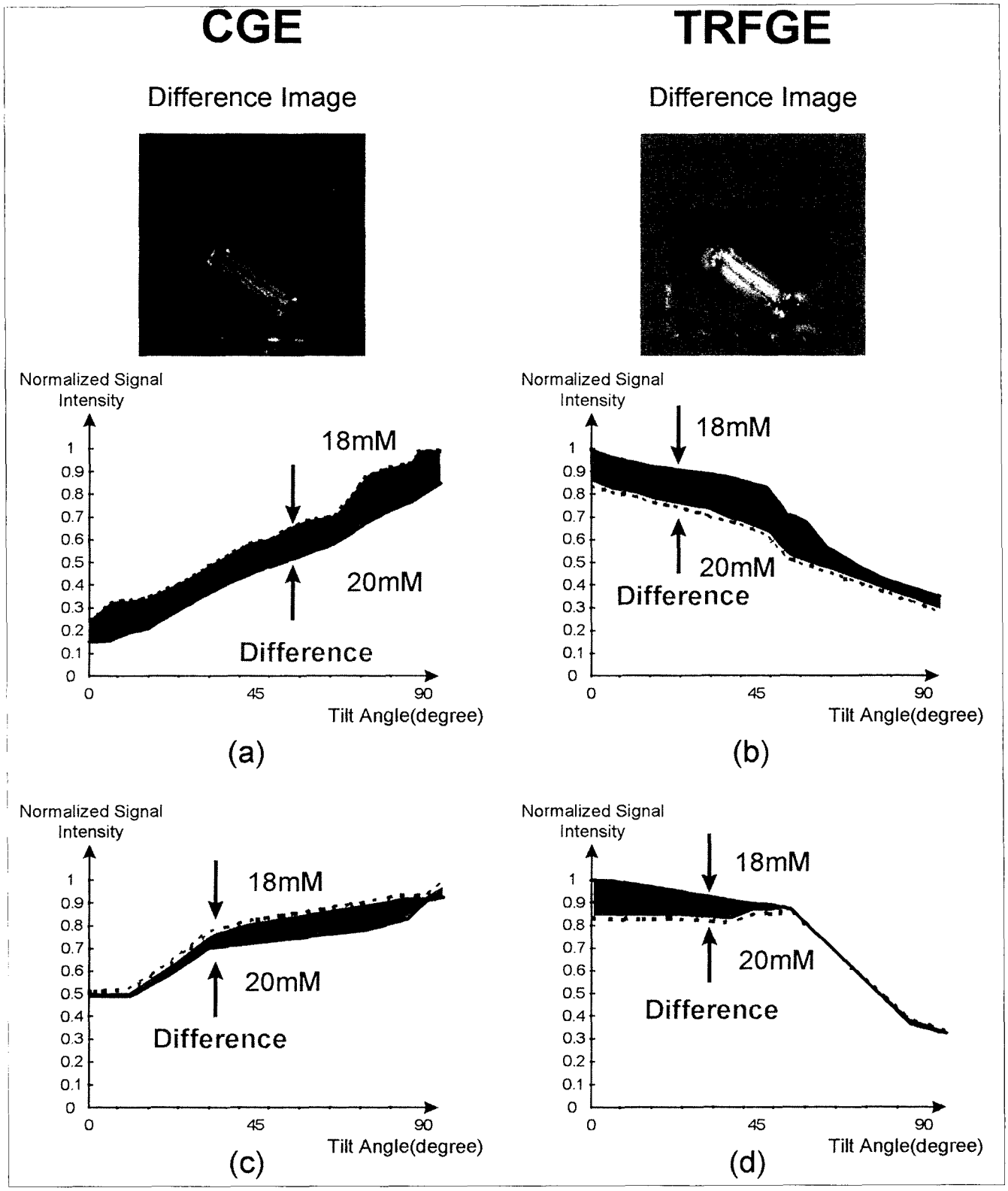

Fig. 8. The normalized signal intensity curves obtained from 15mm and 10mm diameter tube bundles with varying the tilting angles against the main magnetic field B_0 for the two Gd—DTPA solutions (18mM and 20mM). Data obtained from the CGE sequence (**a** & **c**). Data obtained from the TRFGE sequence (**b** & **d**).

7). The experimental phantom also consists of two capillary bundles of two different susceptibility values, namely 20mM and 18mM Gd−DTPA solutions, respectively, as shown in Fig. 7. The resulting susceptibility difference indicates a corresponding value of 0.05ppm. Imaging parameters were TR/TE =40/25msec, flip angle $\alpha=30^{\circ}$ and slice thickness= 10mm. Fig. 8 show experimental data of sagittal images obtained from the 15mm and 10mm diameter bundles with the CGE and TRFGE sequences, respectively for the two Gd−DTPA solutions (18mM and 20mM) with varying the tilting angles. Fig. 8(a) and (b) show the signal intensity changes and difference of the set in the 15mm diameter bundles as a function of the tilting angle for the CGE and TRFGE, respectively. Signal intensity changes in the 10mm diameter bundles as a function of the tilting angle are also shown in Fig. 8(c) and (d) for the two Gd−DTPA solutions. Although there are some differences between the large capillaries (1mm tubes) and small capillaries (300μm tubes) bundles, the trend of signal intensity variation appears same for the two cases. The signal intensity as well as the differences has the tendency of decreasing with increasing tilting angle for the TRFGE sequence while for the CGE the trends were opposite.

Discussion and Conclusions

For the quantitative understanding of the "BOLD" effect, it was necessary to examine various factors, namely imaging modes (sagittal, axial, coronal), assumptions of vessel layouts (line tilt angles of the vessels and capillaries or bundle of the capillaries), and also the pulse sequences employed. It was found that the maximum "BOLD" sensitivity seems obtainable with the sagittal imaging. For the parallel capillary bundles of two different sizes clearly show the difference in intensities as a function of tilt angles (see Fig. 8(a) and (b)). The differences, however, was relatively insensitive to the tilt angles. Two examples of gradient echo sequences (CGE and TRFGE) show similar difference sensitivities (20mM to 18mM) with an opposite trend, however, TRFGE appears less sensitive to the tilt angle showing relatively constant differences till $\theta=60^{\circ}$. Present study also suggested that the pulse sequence such as the TRFGE sequence clearly superior to the conventional BOLD sensitive techniques such as the conventional gradient echo (CGE) sequence, the later (TRFGE) not only shows superior contrast sensitivity over CGE but also insensitive to inflow effect as well as bulk susceptibility effect which undesirable information of measuring the capillaries and distinguishing the capillaries from that of the large venous vessels (see Figs. 4 and 5).

References

1. Kwong KK, Belliveau JW, Chesler DA, et al. Dynamic magnetic resonance imaging of human brain activity during primary sensory stimulation. Proc Natl Acad Sci (USA), 1992;89:5675-5679
2. Ogawa S, Lee TM, Kay AR, Tank DW. Brain magnetic resonance imaging with contrast dependence on blood oxygenation. Proc Natl Acad Sci (USA), 1990;87:9868-9872
3. Tunner R, Jezzard P, Wen H, et al. Functional mapping of the human visual cortex at 4 and 1.5 tesla using deoxygenation contrast EPI. Magn Reson Med 1993;29: 277-279
4. Frahm J, Merbolt KD, Hanicke W. Functional MRI of human brain activation at high spatial resolution. Magn Reson Med 1993;29:139-144
5. Bandettini PA, Wong EC, Hinks RS, Tikfsky RS, Hyde JS. Time course EPI of human brain function during task activation. Magn Reson Med 1992;25:390-397
6. Haacke EM, Hopkins A, Lai S, et al. 2D and 3D high resolution gradient echo functional imaging of the brain: venous contributions to signal in motor cortex studies. NMR Biomed 1994;7:54-62
7. Kim SG. Quantification of Relative Cerebral Blood Flow Change by Flow-Sensitive Alternating Inversion Recovery (FAIR) Technique: Application to Functional Mapping. Magn Reson Med 1995;34:293-301
8. Constable RT, McCarthy G, Allison T, Snderson AW, Gore JR. Functional brain imaging at 1.5 Tesla using conventional gradient echo imaging techniques. Magn Reson Imaging 1993;11:451-459
9. Noll DC, Meyer CH, Cohen JD, Schneider W. Spiral scan imaging of cortical activation. in Proc., SMR, 12th Annual Meeting, San Francisco, 1993;44
10. Turner R, Jezzard P, Wen H, et al. Functional mapping of the human visual cortex at 4 and 1.5 Tesla using deoxygenation contrast EPI. Magn Reson Med 1993;29: 277-279
11. Moonen CTW, Liu G, Gelderen P, Sobering GA. A fast gradient - recalled MRI technique with increased sensitivity to dynamic susceptibility effects. Magn Reson Med 1992;26 :184-189
12. Cho ZH, Ro YM, Park JB, Chung SC, Park SH. Functional brain imaging using blood flow changes. Proc SMRM 12th Annual Meeting, 1993;170
13. Cho ZH, Ong RL, Ro YM, Chung SC, Park SH, Park JB. Susceptibility and Flow Effects in Functional MR Imaging

Using Tailored RF Pulse. IEEE Conf Rec Nucl Sci & Med Imag Simposium 1993;3:1480-1484
14. Cho ZH, Ro YM, Park SH, Chung SC, Ong R. NMR functional imaging using tailored RF gradient echo sequence - a true susceptibility measurement technique. Proc SMR 1994; 659
15. Cho ZH, Ro YM, Chung SC. Susceptibility effect-enha-nced functional MR imaging using tailored RF gradient echo (TRFGE) sequence. Int J Imag Sys Tech 1995;6:164-170
16. Cho ZH, Ro YM, Park SH, Chung SC. NMR Functional Imaging Using A Tailored RF Gradient Echo Sequence:A True Susceptibility Measurement Technique. Magn Res Med 1996;35:1-5
17. Thulborn KR, Waterton JC, Mathews PM, George R. Oxygenation Dependence of the Transverse Relaxation Time of Water Protons in Whole Blood at High Field. Biochim Biophy Acta 1982;714:265-270
18. Stryer L. Biochemistry. 2nd ed. W.H. Freman and Company, New York, 1981
19. Kennan RP, Zhong J, Gore JC. Intravascular Susceptibility Contrast Mechanisms in Tissues. Magn Reson Med 1994;31 :9-21

대한자기공명의과학회지 1:66-74(1997)

뇌기능 영상을 위한 TRFGE와 CGE 기법에서 자화율 효과의 정량적 해석

[1]한국과학 기술원 전기 및 전자공학과
[2]대전대학교 컴퓨터 공학과

정순철[1], 노용만[2], 조장희[1]

혈액의 산소화와 불 산소화에 따른 국부적인 자화율 효과의 변화에 의한 자장의 불 균일성에 민감한 경사 자장 에코 기법은 현재의 뇌기능 MR 영상의 기본이 되고 있다. 일반적으로 이러한 경사 자장 에코 기법은 T2* 혹은 BOLD 효과에 의한 자장의 불 균일성의 증가가 신호의 감소로 나타난다. BOLD 효과는 주자장에 대한 핏줄의 방향이나 영상 형식, 즉, 횡단면, 관상면, 또는 시상면에 따라 달라진다. 그래서 영상 형식과 영상면에 대한 기울임 각에 따른 신호의 변화와 BOLD 효과의 변화에 대한 정량적인 연구를 하였다. 연구는 자화율 효과에 대해 다른 민감도를 가지는 TRFGE와 CGE 기법으로 이루어 졌다. 컴퓨터 모의 실험과 실험 결과를 본 논문에 나타내었다.

통신저자 : 정순철 서울시 동대문구 청량리동 207-43 한국과학기술원 전기 및 전자공학과
Tel. 82-2-958-3352 Fax. 82-2-965-4394